Chemical Engineering Journal 166 (2011) 669–677

Contents lists available at ScienceDirect

Chemical Engineering Journal

journal homepage: www.elsevier.com/locate/cej

Membrane fouling mechanism and concentration effect in cross-flow microfiltration of BSA/dextran mixtures

Kuo-Jen Hwang*, Pan-Yu Sz

Department of Chemical and Materials Engineering, Tamkang University, Tamsui, Taipei Hsien 25137, Taiwan

ARTICLE INFO

Article history:
Received 28 June 2010
Received in revised form 8 November 2010
Accepted 11 November 2010

Keywords:
Cross-flow microfiltration
Membrane fouling
Membrane filtration
Bio-separation

ABSTRACT

Membrane fouling in BSA/dextran binary suspension cross-flow microfiltration under various operating conditions is studied. The mechanisms for membrane fouling based on the SEM and CSLM observations under various suspension concentrations are proposed. BSA aggregates deposit onto the membrane surface while dextran molecules adsorb into the membrane pores, resulting in filtration resistances. The BSA deposition is mainly determined by the drag forces exerted on BSA aggregates on the membrane surface. Dextran adsorption is affected by the dextran concentration and applied pressure. The concentration effects on the filtration flux and filtration resistance are also discussed. The filtration fluxes for BSA/dextran mixtures are located between those for two pure substances and decrease with the increase in either the BSA or dextran concentration. However, the dextran concentration impact is more significant because the filtration resistance caused by membrane blocking is much higher than that caused by cake formation in most conditions. The filtration resistances due to concentration polarization, cake formation and membrane internal fouling can be estimated directly from the operating conditions using the semi-theoretical methods proposed in this study.

1. Introduction

Membrane filtration has been widely used in the separation and purification of biological products in biotechnology. This is because it could have the advantages of high product selectivity, high separation efficiency and high system integration flexibility through optimum membrane selection and module design. However, membrane fouling during a filtration may markedly reduce the filtration flux, decrease product quality and consequently increase the operating costs. Alleviating membrane fouling is therefore the most important course to achieve optimum operations. Membrane fouling in membrane filtration is possible due to solute adsorption, particle deposition, membrane blocking, or concentration polarization [1]. Because multiple components, such as microbial cells, proteins, polysaccharides, or humic acids, always coexist in biological products, the membrane fouling mechanisms are complex and dependent on the physical and chemical characteristics of foulant and membrane. Thus, the fouling mechanisms caused by different foulants, especially by bio-mixtures with different compositions, have not been well analyzed yet.

Many factors, such as membrane characteristics, particle or solute properties, operating conditions, etc., affect membrane fouling during a filtration [1]. In previous studies on the membrane filtration of pure Bovine Serum Albumin (BSA), Tracey and Davis [2] and Bowen et al. [3] indicated that the membrane pore size and BSA concentration played important roles in membrane fouling in microfiltration. The membrane fouling type changed from internal blocking into cake formation after a period of filtration. Huisman et al. [4] claimed that the interaction between BSA and membrane determined the early stage membrane fouling, while the later period performance of the cross-flow ultrafiltration was dependent on the BSA interactions. Güell and Davis [5] studied the ultrafiltration of protein mixtures using four kinds of membranes. The membrane fouling was attributed to the interactions between protein functional groups. Ouammou et al. [6] concluded that the protein zeta potential was the most important factor affecting membrane fouling in protein microfiltration. Iritani et al. [7] studied the ultrafiltration of protein mixtures including BSA and egg white lysozyme. They also concluded that the protein electrostatic interactions played an important role in determining membrane fouling and filtration flux. Reducing cake formation using high shear stresses or vortex flows was demonstrated as an efficient method to enhance separation efficiency in the filtration of protein mixtures [1,8].

Different approaches were also proposed in previous studies. Blatt et al. [9] claimed that membrane fouling in protein ultrafiltration could be divided into two pressure-dependent regimes. The polarization concentration increased with increasing pressure in the low pressure region, while a gel layer formation or a reduction in membrane pore size occurred under high pressures.

* Corresponding author. Tel.: +886 2 26215656x2726; fax: +886 2 26209887.
E-mail address: kjhwang@mail.tku.edu.tw (K.-J. Hwang).

1385-8947/$ – see front matter © 2010 Elsevier B.V. All rights reserved.
doi:10.1016/j.cej.2010.11.044

Nomenclature

C	solute concentration in the bulk suspension (kg/m^3)
C_2	correction factor defined in Eq. (10)
D	molecular diffusivity (m^2/s)
d_h	hydraulic diameter of filter channel (m)
$d_{m,o}$	clean membrane pore diameter (m)
$d_{m,b}$	fouled membrane pore diameter (m)
d_p	diameter of particle (BSA aggregates) (m)
F_n	drag force in normal (filtration) direction (N)
F_t	drag force in tangential (cross-flow) direction (N)
H	clearance of filter channel (m)
k	mass transfer coefficient (m/s)
L	cake thickness (m)
L_f	length of filter channel (m)
MW	molecular weight (Da)
q	filtration flux (m^3/m^2 s)
q_s	pseudo-steady filtration flux (m^3/m^2 s)
Re	Reynolds number
R_c	filtration resistance due to filter cake (m^{-1})
R_{cp}	filtration resistance due to concentration polarization layer (m^{-1})
R_{if}	filtration resistance due to membrane internal fouling (m^{-1})
R_f	filtration resistance due to membrane fouling (m^{-1})
R_m	filtration resistance of clean membrane (m^{-1})
R_t	total filtration resistance (m^{-1})
Sc	Schmidt number
Sh	Sherwood number
t	filtration time (s)
u_s	cross-flow velocity (m/s)
w_c	cake mass (kg/m^2)

Greek letters

α_{av}	average specific cake filtration resistance (m/kg)
ε_{av}	average cake porosity
δ	thickness of fouling layer in the membrane pores (m)
ΔP	filtration pressure (Pa)
γ_o	shear rate on the membrane surface (s^{-1})
μ	filtrate viscosity (kg/s m)

Subscripts

B	BSA
D	dextran

Moreover, the gel-polarization model was proposed for correcting the formation of a gel layer on the membrane surface other than a sole concentration polarization [10]. The filtration resistance in dextran ultrafiltration was then accurately predicted using this model [11]. Based on the mass transfer concepts, the concentration polarization or gel layer resistance could be efficiently reduced by increasing the cross-flow velocity [10,11]. Garcia-Molina et al. [12] studied the ultrafiltration of dextran suspensions. They indicated that a fouling layer was always formed and the filtration flux was increased by increasing filtration pressure. In the cross-flow microfiltration of red wine, Vernhet and Moutounet [13] found that the polysaccharides in red wind were the major foulants. Membrane fouling frequently occurred at the membrane pore entrances or on the membrane surface. Recently, Hwang and Huang [14] concluded that the membrane pore size reduction caused by dextran adsorption was the main membrane fouling type in the cross-flow microfiltration of blue dextran. From the results in previous studies, the filtration flux in protein/polysaccharide mixture microfiltration was much lower than that containing only a single component [15,16]. Susanto et al. [15] found that the fouled layer morphology was markedly dependent on the polysaccharide characteristics and was more compact compared to that formed by pure proteins. Hwang and Sz [16] studied the membrane fouling in cross-flow microfiltration of BSA/dextran binary suspensions. They found that the membrane fouling was mainly due to dextran adsorption into the membrane pores. The fouled membrane pore size and fouled layer thickness under various conditions could be estimated using a theoretical model based on the Hagen–Poiseuille law.

In this study, membrane fouling causing by BSA/dextran mixtures in cross-flow microfiltration is studied. The membrane fouling observed using SEM and CSLM under various suspension concentrations is modeled in order to propose fouling mechanisms. The filtration resistances causing by the deposition of BSA aggregates onto the membrane surface and by the adsorption of dextran molecules in the membrane pores are analyzed. The concentration effects on the filtration flux and resistance are also semi-theoretically discussed according to the membrane fouling mechanisms.

2. Materials and methods

BSA with a molecular weight of 67 kDa was purchased from United State Biochemical Co., while the dextran used in these experiments was manufactured by Sigma Chemical Co. in the USA with a mean molecular weight of 2000 kDa. BSA and dextran were dissolved in a 10 mM phosphate buffer solution to prepare suspensions with different concentrations. The suspension pH and temperature during filtration were set at 7.0 and 20 °C, respectively. The suspension was continuously stirred for 1 h to reach a steady-state of BSA aggregate formation. The BSA and dextran sizes were measured using *Malvern MRK528-01 Zetasizer Nano System* and are shown in Fig. 1. Although BSA molecules had a primary size of 8 nm, many aggregates with a size as large as 300 nm were found in the suspension. Dextran had a size distribution from 21 to 300 nm and a mean value of 90 nm. The BSA aggregation was observed to be insignificantly affected by dextran concentration in the operating conditions of this study by checking the size distribution. A hydrophilic flat-sheet membrane made of mixed cellulose acetate, manufactured by Millipore Co., USA (Cat. No.: VCWP14250), was used in these experiments. The membrane possessed good BSA

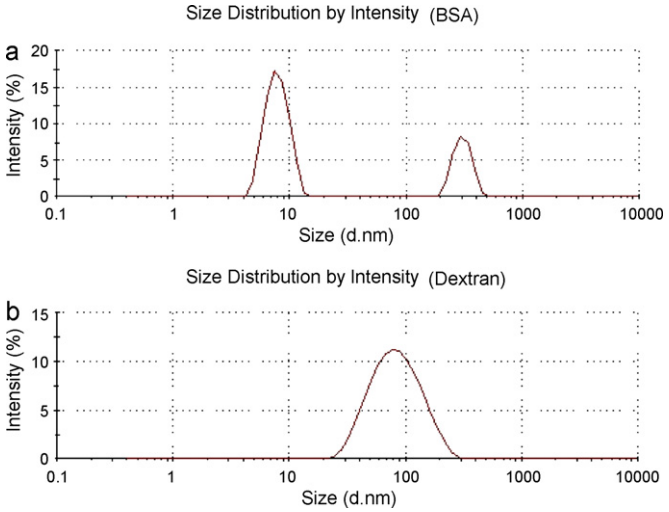

Fig. 1. Size distributions of (a) BSA, and (b) dextran.

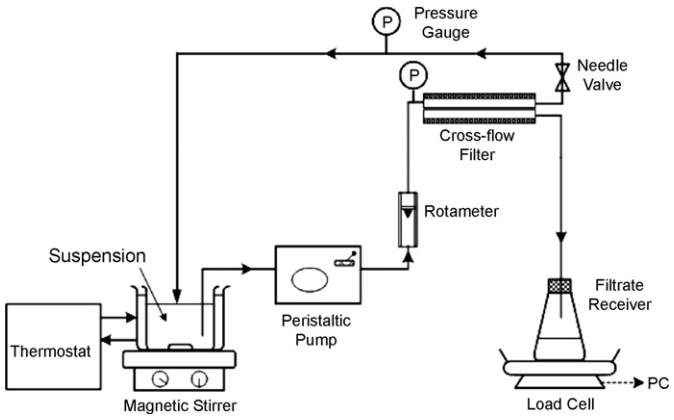

Fig. 2. A schematic diagram of the cross-flow microfiltration system.

rejection property. The mean pore diameter on the virgin membrane surface was measured at 295 nm using a *Power Image Analysis System*.

A schematic diagram of the cross-flow microfiltration system is shown in Fig. 2. The clearance, width and length of the effective filtration region in the two-parallel-plate micro-filter were 1.0×10^{-3} m, 2.0×10^{-2} and 5.5×10^{-2} m, respectively. Only the bottom plate was permeable and installed with a filter membrane. The suspension was prepared in a suspension tank, agitated using a magnetic mixer and kept isothermal using a thermostat. The suspension was pumped into the microfilter using a *Millipore 7518-00 Peristaltic Pump*. The measured results of protein size distributions indicated that the protein aggregation was not obvious change by the pumping shear. The cross-flow velocity and filtration pressure were adjusted using a rotameter and a needle valve, respectively. The concentrate was pumped back to the suspension tank, while the filtrate was collected into a flask and weighed using a load cell. The filtration data were then recorded on a personal computer for further calculation. When an experiment was terminated, the filtrate viscosity was measured using *Brookfield LVDV-II* viscometer. The fouled membrane was sent to perform Scanning Electron Microscopy (SEM) using *Leo-1530 Field Emission Scanning Electron Microscopy* or Confocal Scanning Laser Microscopy (CSLM) using *Leica TCS-SP5 Confocal Spectral Microscope Imaging System*. In CSLM analysis, the selected fluorescent dyes for BSA and dextran were Fluorescein-5-Isothiocyanate FITC "Isomer I" (FITC) and Concanavalin A-Tetramethylrhodamine Conjugate (ConA), respectively.

The sources of filtration resistances included concentration polarization layer, membrane fouling and the virgin membrane. These resistances were measured in experiments. The virgin membrane resistance was measured before each experiment by flowing de-ionized water through the membrane, while the overall filtration resistance was calculated by substituting filtration flux and pressure data into the basic filtration equation. As soon as an experiment was completed, the suspension flow was switched instantaneously to de-ionized water. Because the concentration polarization layer was swept away from the region near the membrane surface, the filtration flux was suddenly increased, and the filtration resistance caused by concentration polarization layer was calculated from the difference between the overall filtration resistance before and after changing feeds. The dextran desorption from membrane pores in such a short period was negligible. The resistance caused by membrane fouling was then calculated using the basic filtration equation once the other resistances were obtained.

3. Results and discussion

Fig. 3(a)–(h) shows SEM photos of the membranes fouled by different concentrations of BSA/dextran mixtures after 3-h filtration under $u_s = 0.3$ m/s and $\Delta P = 60$ kPa. The top- and side-view of the membrane fouled by pure BSA with a concentration of 1 kg/m^3 are shown in Fig. 3(a) and (b), respectively. Fig. 3(a) illustrates that some BSA aggregates several hundred nanometers in size are retained on the membrane surface, forming a filter cake. The "gel-like" cake layer is rather compact compared to those formed by incompressible particles (e.g., glass beads, metal powders or some polymeric particles) with a similar size. However, a few membrane pores remained open on the surface after 3-h filtration. The side-view of the fouled membrane, Fig. 3(b), indicates that the BSA fouled layer is very thin (only several hundred micrometers) with no BSA molecule adsorbed into the walls of the membrane pores. These phenomena reveal that the resistance in pure BSA filtration is due mainly to the thin cake layer formed on the membrane surface.

Fig. 3(c)–(h) is images of membranes fouled by BSA/dextran mixtures with different concentrations. Fig. 3(c) and (d) shows the top- and side-view, respectively, of the fouled membrane under $C_B = 1$ kg/m^3 and $C_D = 0.5$ kg/m^3. BSA aggregates with an approximate size of 300 nm form a "spot-like" thin cake layer on the membrane surface. Only a part of the membrane surface area is covered with deposited BSA after 3-h filtration. Some dextran molecules are found to adsorb onto the sponge-like interior membrane pores near the pore entrances. The membrane pores are narrowed due to the dextran adsorption, which results in a significant filtration resistance. When the dextran concentration was doubled, the BSA cake structure and thickness were nearly the same, as shown in Fig. 3(e) and (f). However, more dextran molecules were found to adsorb into the membrane pores under such higher dextran concentration. Because this effect causes the pore size of the fouled membrane to be smaller, the filtration resistance is expected to increase noticeably. When the BSA concentration was doubled but C_D remains as 0.5 kg/m^3, most of the membrane surface area is covered with BSA aggregates, while the cake thickness is still thin after 3 h, as shown in Fig. 3(g) and (h). The aggregate size increases to 1–2 μm and the shape changes to spheroidal in higher BSA concentration conditions. Because the dextran adsorption was similar under the same dextran concentration, as shown in Fig. 3(d) and (h), the increase in overall filtration resistance with increasing BSA concentration is mainly attributed to more BSA deposition.

Applying fluorescent dye to fouled membrane sampling, BSA and dextran in CSLM can be observed in green and red colors, respectively. The results of pure BSA and dextran under a dead-end filtration of $\Delta P = 20$ kPa are shown in Fig. 4(a) and (b) as blanks. Fig. 4(c) and (d) shows typical photos of CSLM under $C_B = 1$ kg/m^3, $C_D = 0.5$ kg/m^3 and $u_s = 0.1$ m/s. The filtration pressures in Fig. 4(c) and (d) are 20 kPa and 100 kPa, respectively. It can be seen that the color on most of the membrane surface is green. This reveals that BSA is the main constituent of the foulant on the membrane surface. Furthermore, the green fluorescence is more intense and can be detected in deeper locations under higher filtration pressure, as those cross-sections shown on the right and bottom of Fig. 4(c) and (d). This indicates that the BSA foul layer is thicker under higher pressure.

According to the SEM and CSLM discussions on fouled membranes shown in Figs. 3 and 4, a composite mechanism constituting cake formation and membrane pore blocking is proposed to explain the membrane fouled by BSA/dextran binary mixtures with different concentrations, as shown in Fig. 5. In the filtration of pure BSA, BSA aggregation always occurs in the suspension [17,18]. The BSA aggregates will be retained on the membrane surface to form a thin but compact cake layer, as shown in Fig. 5(a). The fil-

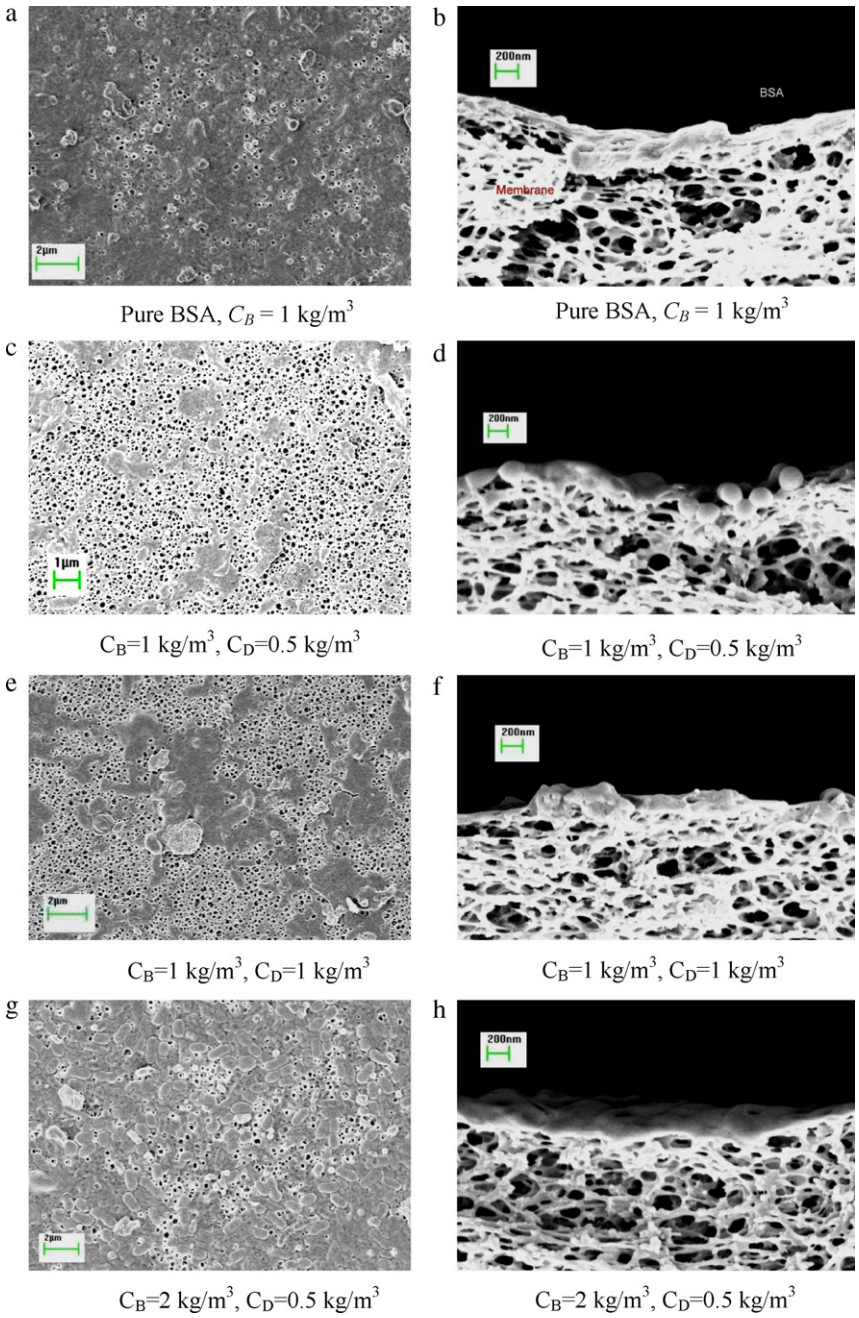

Fig. 3. SEM photos for the fouled membrane under u_s = 0.3 m/s and ΔP = 60 kPa. (a and b) Pure BSA, C_B = 1 kg/m^3, (c and d) C_B = 1 kg/m^3, C_D = 0.5 kg/m^3, (e and f) C_B = 1 kg/m^3, C_D = 1 kg/m^3, (g and h) C_B = 2 kg/m^3, C_D = 0.5 kg/m^3.

tration resistance caused by cake formation is dominant in such condition. When dextran molecules co-exist in the suspension, they have the opportunity to be adsorbed into the membrane pores. Referring to the SEM shown in Fig. 3 and the analysis in the authors' previous study [16], the dextran adsorption occurs at the membrane pore entrances, leading to a reduction in the pore size as well as an increase in filtration resistance, as shown in Fig. 5(b). Because a lower filtration flux causes BSA aggregates to deposit on the membrane surface more difficulty, the BSA cake layer only covers a part of the membrane surface and has a thickness merely several times the size of a BSA aggregate. Therefore, the filtration resistance for BSA/dextran mixtures is mostly attributed to the pore size reduction by dextran adsorption. The dextran adsorption layer is thicker under higher dextran concentrations, as shown in Fig. 5(c). This implies that the filtration resistance increases with increasing dextran concentration for a given BSA concentration under fixed cross-flow velocity and filtration pressure.

Fig. 6 shows the filtration flux attenuation during cross-flow microfiltration of BSA/dextran mixtures with different concentrations. The cross-flow velocity and filtration pressure are kept at 0.3 m/s and 100 kPa, respectively, during filtration. Similar to those in most cross-flow microfiltration systems, the filtration fluxes attenuate very quickly at the beginning of filtration and gradually approach pseudo-steady values after a period of time. This trend reveals that most membrane fouling occurs in the early filtration period. Since the filter cake formed by BSA has a thickness only approximately several times that of a BSA aggregate, the aggregate deposition may occur in very early filtration periods. This fact causes the filtration flux to decay more quickly under higher BSA

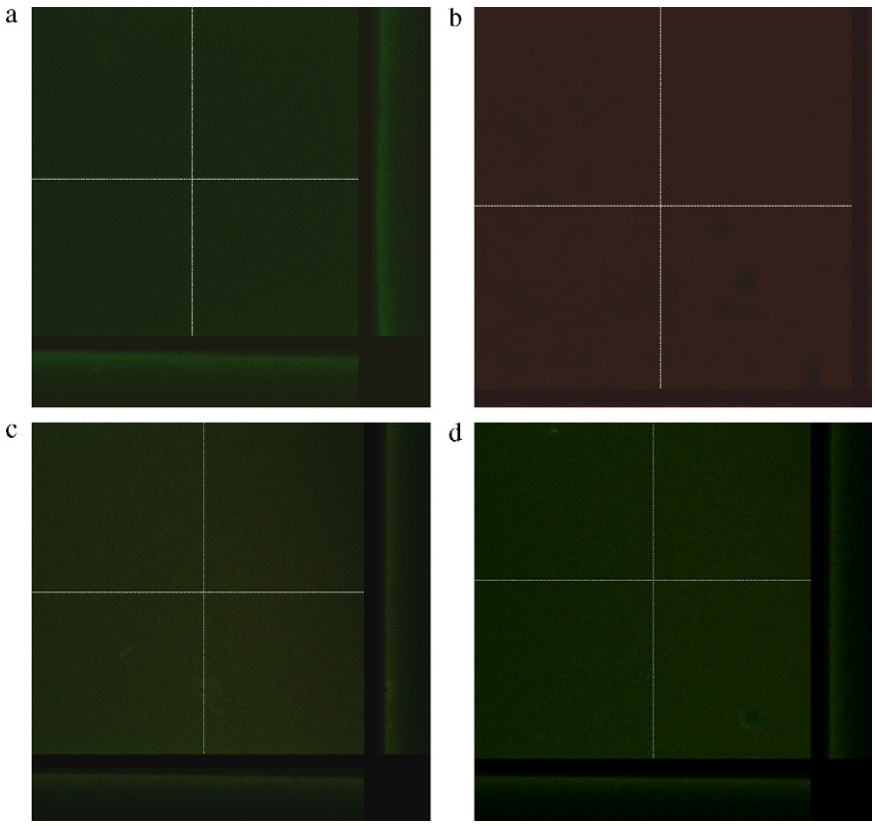

Fig. 4. The 3D reconstruction of CSLM image stacks (10 × 100×) under C_B = 1 kg/m^3, C_D = 0.5 kg/m^3, (a) pure BSA, u_s = 0 m/s, ΔP = 20 kPa, (b) pure dextran, u_s = 0 m/s, ΔP = 20 kPa, (c) mixture, u_s = 0.1 m/s, ΔP = 20 kPa, and (d) mixture, u_s = 0.1 m/s, ΔP = 100 kPa.

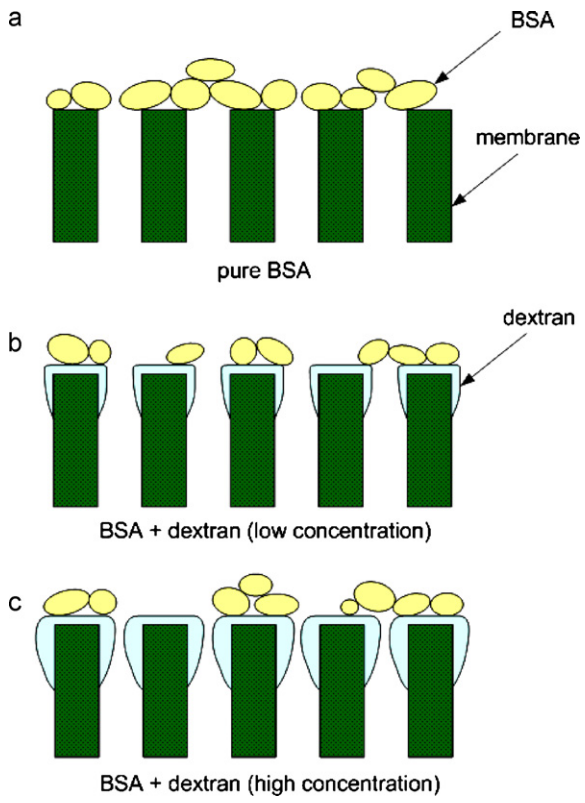

Fig. 5. Schematic diagram for the mechanisms of the membrane fouled by BSA/dextran mixtures with different concentrations. (a) Pure BSA, (b) BSA + dextran (low concentration), and (c) BSA + dextran (high concentration).

concentration, i.e., C_B = 2 kg/m^3. Comparing the data shown in Fig. 6, the filtration flux would be the highest in pure BSA suspension filtration. This is because the filtration resistance is solely due to cake formation. When dextran molecules exist in the suspension, the dextran adsorption causes the membrane pore size to reduce as well as a filtration resistance increase. As a result, the filtration flux decays quicker at the initial stage and decreases with increasing dextran concentration. Comparing the data from a solid circle and square, it is inferred that the lower flux for higher BSA concentration before 1000 s is caused by more BSA aggregate deposition, while the lower steady flux for higher dextran concentration after

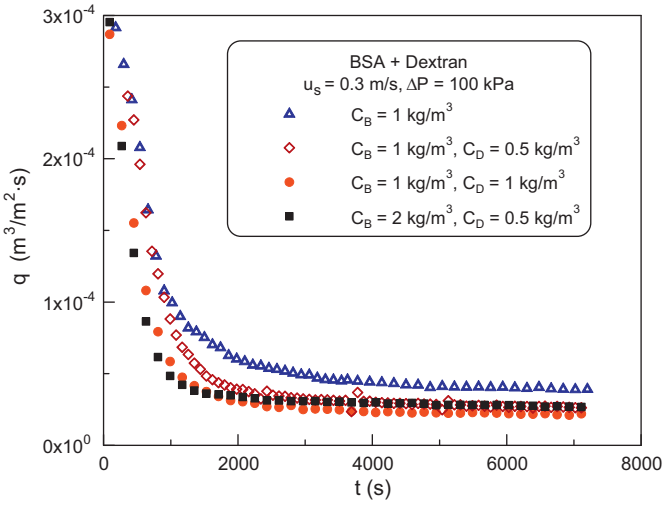

Fig. 6. The filtration flux attenuations during cross-flow microfiltration of BSA/dextran mixtures with different concentrations.

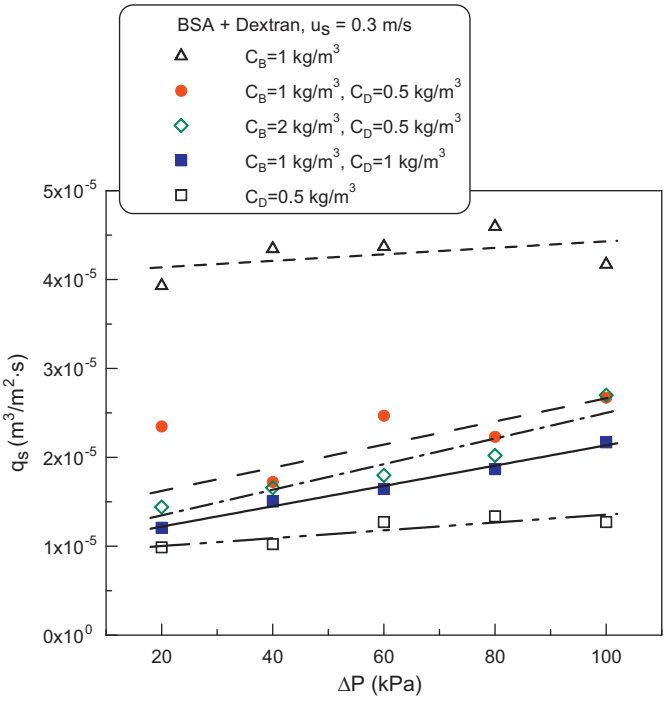

Fig. 7. Effects of suspension concentration and filtration pressure on the pseudo-steady filtration flux.

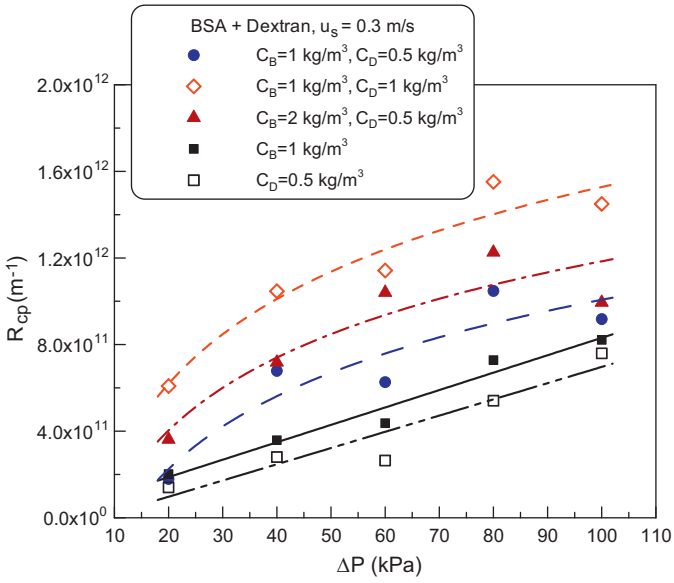

Fig. 8. Pressure effect on the R_{cp} value for different mixed BSA/dextran compositions.

that time is due to more dextran adsorption into the membrane pores.

Fig. 7 shows the suspension concentration and filtration pressure effects on the pseudo-steady filtration flux. The cross-flow velocity is fixed at 0.3 m/s. According to the membrane fouling mechanism shown in Fig. 5, BSA aggregates deposit onto the membrane surface while dextran molecules adsorb onto the walls of the membrane pores resulting in filtration resistances during filtration. Because the filtration resistance caused by membrane internal fouling is much higher than that caused by cake formation in most conditions, the filtration flux for pure BSA is 4-fold higher than that for pure dextran suspensions. The filtration fluxes for pure components are relatively insensitive to filtration pressure. This implies that the membrane fouling becomes more severe under higher pressure and increasing filtration pressure may not be an efficient strategy to enhance filtration flux. For the filtration of BSA/dextran mixtures, the filtration fluxes are located between that of two pure substances. The fluxes are more sensitive to filtration pressure compared to those of pure suspensions, but it increases less than 2 times when the pressure is increased from 20 to 100 kPa. This is possible due to the competition of two constitutive membrane fouling mechanisms, cake formation and membrane pore blocking. Comparing the filtration fluxes for those mixtures with different concentrations, it can be found that the flux decreases with the increase in BSA or dextran concentration. However, the impact of dextran concentration is more significant.

The basic filtration equation based on resistance-in-series model can be written as:

$$q = \frac{\Delta P}{\mu R_t} = \frac{\Delta P}{\mu(R_{cp} + R_f + R_m)} \quad (1)$$

where q is filtration flux, ΔP is filtration pressure, μ is filtrate viscosity, and R_t is the overall filtration resistance which can be given by summing the filtration resistances caused by concentration polarization layer, R_{cp}, membrane fouling, R_f, and the virgin membrane, R_m. The methods for filtration resistance measurements have been described in previous section. Because the existence of BSA and dextran in the filtrate causes a 2–10% increase in viscosity, the filtrate viscosity should be measured and used in resistance calculation. Fig. 8 shows the pressure effect on the R_{cp} value for different mixed BSA/dextran concentrations. An increase in filtration pressure leads to higher R_{cp} value for a given suspension concentration. The R_{cp} value for pure BSA is lower than that for pure dextran. A linear relationship between R_{cp} and ΔP can be found for these two pure substances. This trend is the same as that of pure substances in previous studies, e.g., Cheng et al. [11]. However, the linear relationship does not exist for the mixtures, and some R_{cp} values for mixtures exceed the sum of two pure substances. This is because BSA and dextran molecules have different mass transfer properties and filtration resistances even under a given operating condition, which will be discussed later. From the experimental data, however, the R_{cp} value increases with increasing BSA or dextran concentration, but the impact of the dextran concentration is more significant.

Analogizing with heat transfer for laminar flow through a channel, an empirical equation to relate Sherwood number, Sh, and other dimensionless groups can be expressed as [10]:

$$Sh = \frac{k \cdot d_h}{D} = 1.86 Re^{0.33} Sc^{0.33} \left(\frac{d_h}{L_f}\right)^{0.33} \quad (2)$$

where k is the mass transfer coefficient, d_h is the hydraulic diameter of the channel, D is the macromolecular diffusivity, Re is Reynolds number, Sc is Schmidt number, and L_f is the channel length. Consequently, the mass transfer coefficient can be estimated using Eq. (2) once the molecular diffusivity and other operating variables are known. The diffusivity can be estimated using the Einstein equation or some available empirical equations. For instance, the BSA diffusivity is calculated by Stokes–Einstein equation as 5.91×10^{-11} m^2/s based on the mean size of BSA [19], while the dextran diffusivity, D_D, can be estimated using the following empirical equation [20]:

$$D_D = 2.8 \times 10^{-9} \cdot MW^{-0.401} \quad (3)$$

in which MW is the molecular weight of dextran. Therefore, the diffusivity of dextran used in this study is *ca.* 8.326×10^{-12} m^2/s.

According to the principles of transport phenomena, the convection mass flux and the back diffusion mass flux in the filtration

direction are theoretically proportional to $C \times q_s$, and $C \times k$, respectively. In fact, the prediction of the filtration resistance caused by the concentration polarization layer from operation parameters is rather difficult. However, it is reasonable to assume that R_{cp} is in proportion to the polarized solute concentrations and is a linear function of $C \times q_s/k$ for a pure substance. The following empirical equations can be regressed using the experimental data of cross-flow microfiltration of pure BSA and dextran suspensions with different concentrations (not shown), respectively:

$$R_{cp,B} = 8.96 \times 10^9 C_B \cdot q_s/k_B \quad (4)$$

$$R_{cp,D} = 8.14 \times 10^{10} C_D \cdot q_s/k_D \quad (5)$$

When filtration is operated in the pressure control region, the filtration flux linearly increases with increasing filtration pressure. Thus, the filtration resistance caused by concentration polarization layer is always proportional to filtration pressure under fixed suspension concentration and cross-flow velocity. This trend is found in Fig. 8 and just fit with the experimental results of previous studies, e.g., Cheng et al. [11]. Therefore, the R_{cp} values for pure BSA and dextran under a given condition can be estimated using Eqs. (4) and (5), respectively, once q_s is measured in experiment and k is calculated using Eq. (2).

When two components co-exist in the suspension, the contributions came from both components should be considered to obtain the overall R_{cp} value. The empirical equations obtained from pure components, Eqs. (4) and (5) are then summed to obtain the R_{cp} value in mixture filtration by neglecting the solute interactions. Fig. 9 shows a plot of the experimental R_{cp} versus calculated R_{cp} values for different suspension concentrations. The cross-flow velocity is fixed at 0.3 m/s, while the data for a given BSA/dextran composition are obtained under various filtration pressures. The auxiliary straight line means agreement between the experimental and calculated values. The deviations between most experimental R_{cp} and calculated values are smaller than 20% except for a few data points. However, this method provides a convenient way to estimate R_{cp} for mixtures directly from the operating conditions and solute concentrations.

The filtration resistances caused by membrane fouling, R_f, including cake formation and membrane pore blocking, for different mixed BSA/dextran concentrations under various filtration pressures are measured and shown in Fig. 10. It can be found that the R_f values are much higher than the R_{cp} values, as shown in Fig. 8 under the same conditions. This trend agrees with those in most

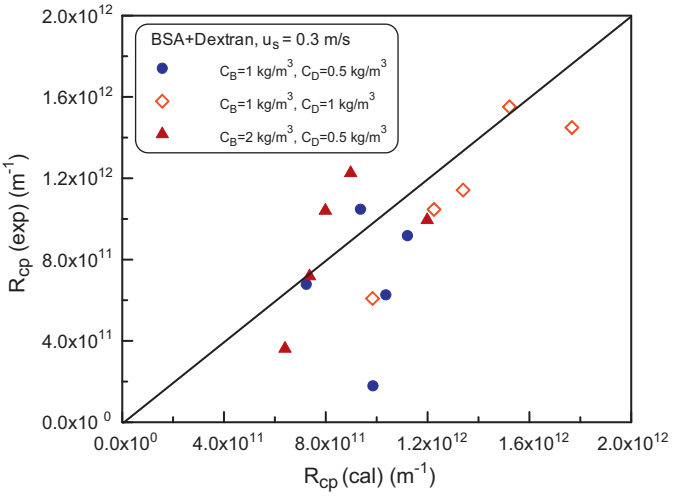

Fig. 9. A plot of experimental R_{cp} versus calculated R_{cp} values for different suspension concentrations.

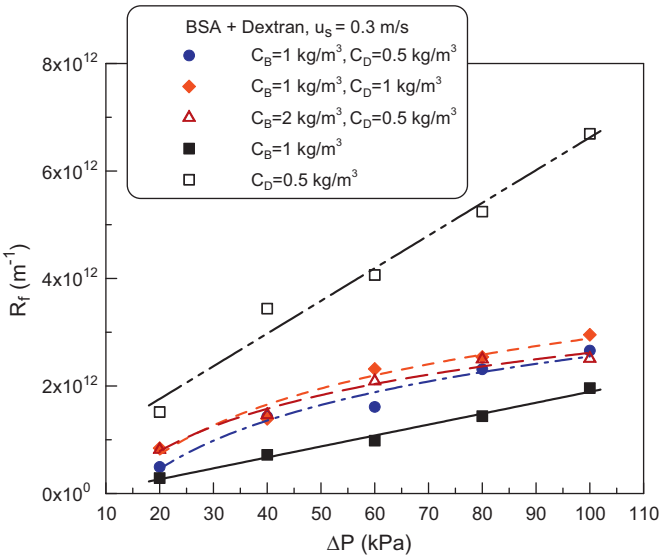

Fig. 10. Effects of BSA/dextran concentrations and filtration pressure on the membrane fouling resistance.

previous studies [1,10,14]. The membrane fouling in pure BSA filtration is due mainly to cake formation, while that in pure dextran filtration is due to sole membrane pore blocking according to the mechanisms proposed by this study. The R_f value for pure BSA is therefore the lowest and that for pure dextran is the highest among the data shown in Fig. 10, and the difference of R_f between two pure substances increases with increasing filtration pressure. Because cake formation may more or less prevent the following membrane pore blocking during BSA/dextran mixture filtration, the R_f values for mixtures are located between those for two pure substances. An increase in the BSA or dextran concentration leads to higher R_f value, but the impact of dextran concentration is more significant.

To understand the weights of cake formation and membrane blocking on fouled membrane filtration resistance in the cross-flow microfiltration of BSA/dextran mixtures, the cake properties in "dead-end" filtration of pure BSA with the same concentrations as this study were measured. The filtration curves were analyzed using the method proposed by Hermia [21] and the results indicated that membrane fouling was attributed to cake formation. The measured average specific cake filtration resistance, α_{av}, and average cake porosity, ε_{av}, can be expressed as the following pressure-dependent power-type empirical equations:

$$\alpha_{av} = 6.22 \times 10^{11} \Delta P^{0.72} \quad (6)$$

$$1 - \varepsilon_{av} = 0.0012 \Delta P^{0.36} \quad (7)$$

Therefore, the cake mass, w_c, under a constant pressure filtration can be estimated from the measured cake filtration resistance, R_c, because $R_c = \alpha_{av} \times w_c$.

In a cross-flow filtration, the deposition of BSA aggregates is restrained by the tangential shear stress due to the suspension flow. Because the fluid velocity near the membrane surface is very low, the tangential drag force exerted on a BSA aggregate staying on the membrane surface can be estimated using the modified Stokes law [22,23], that is,

$$F_t = 2.176\pi\mu d_{p,B}^2 \gamma_o \quad (8)$$

where $d_{p,B}$ is the diameter of BSA aggregate. The shear rate acting on the membrane surface, γ_o, in a two-parallel-plate cross-flow filter can be estimated by [23],

$$\gamma_o = 6\frac{u_s H}{(H-L)^2} = 6\frac{u_s}{H} \quad (\text{when } L \ll H) \quad (9)$$

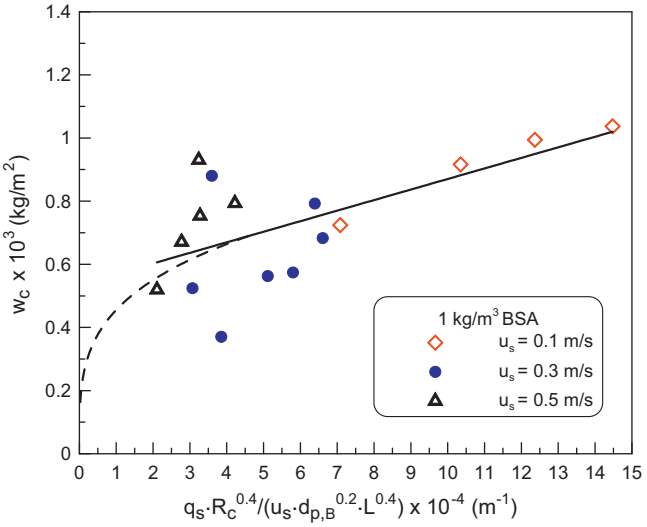

Fig. 11. A plot of calculated cake mass versus $q_s R_c^{0.4}/u_s d_{p,B}^{0.2} L^{0.4}$ in cross-flow filtration of pure BSA suspension under various filtration velocities.

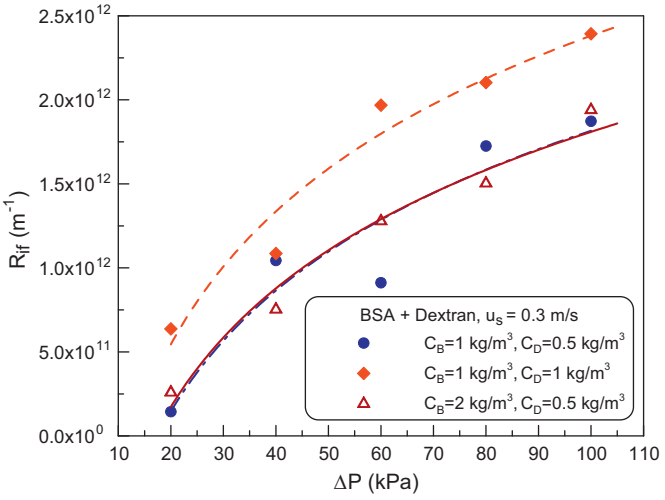

Fig. 12. Effects of BSA/dextran mixture concentrations and filtration pressure on the internal membrane fouling resistance.

where u_s is the mean cross-flow velocity, L is the cake thickness, and H is the clearance of the filter channel. Therefore, $F_t \propto d_{p,B}^2 u_s$ in thin cake conditions. The drag force in the filtration direction can also be calculated using the modified Stokes law:

$$F_n = 3\pi\mu d_{p,B} q_s C_2 \tag{10}$$

The correction factor, C_2, is introduced due to the existence of the filter cake and can be obtained by [24]

$$C_2 = 0.36\left(\frac{R_c d_{p,B}^2}{4L}\right)^{0.4} \tag{11}$$

Therefore, $F_n \propto q_s R_c^{0.4} d_{p,B}^{1.8}/L^{0.4}$. The results in previous studies [22,23] concluded that the particle deposition is determined by the ratio of force in the filtration to that in the tangential (cross-flow) directions. In other words, the force ratio of F_n/F_t, which is proportional to $q_s R_c^{0.4}/u_s d_{p,B}^{0.2} L^{0.4}$, is an important factor affecting the cake formation.

Fig. 11 is a plot of calculated cake mass versus $q_s R_c^{0.4}/u_s d_{p,B}^{0.2} L^{0.4}$ in cross-flow filtration of pure BSA suspension under various filtration velocities. Most data can be regressed to a straight line though a few data have large deviation for about 35% under low force ratios of F_n/F_t. The result reveals that the cake mass increases with increasing the force ratio of F_n/F_t, i.e., increasing the particle stability on the membrane surface. The linear relationship also indicates that the drag forces play the most important role in determining BSA deposition. However, the regressed dash curve under low $q_s R_c^{0.4}/u_s d_{p,B}^{0.2} L^{0.4}$ values deviates from the straight line. This implies that the interaction between BSA aggregates increases its weighting when the drag force due to permeate flow is small. The repulsive interaction due to hydrophobic nature of BSA causes less BSA deposition in such conditions, and this effect becomes more significant under lower force ratios of F_n/F_t.

For the filtration of BSA/dextran mixtures, the cake mass formed by BSA aggregates can be estimated using the empirical relationship shown in Fig. 11, and the cake resistance R_c can be calculated using the product of $\alpha_{av} \times w_c$ in which α_{av} is obtained using Eq. (6). The filtration resistance caused by internal membrane fouling (or says membrane pore blocking), R_{if}, is then calculated by subtracting R_c from R_f values. Fig. 12 shows the calculated R_{if} values for three different BSA/dextran mixture concentrations under various filtration pressures. Because the main contributor on membrane internal fouling is dextran, increasing dextran concentration leads to higher R_{if} value. This effect is more significant under higher filtration pressures. Furthermore, more dextran molecules have opportunities to penetrate into the membrane pores under higher filtration flux, which results in more serious membrane internal fouling under higher pressures. The R_{if} value increases more than 5 times as pressure increases from 20 to 100 kPa. The data shown in Fig. 12 also indicates that the BSA concentration has no obvious effect on the R_{if} value. The membrane internal fouling is mainly determined by the dextran concentration and filtration pressure.

In the authors' previous study [16], the relationship among filtration flux, fouled membrane pore size, and pressure drop through the membrane fouled layer at steady state was modeled by the Hagen–Poiseuille law. The increase in filtration resistance was attributed to the reduction in membrane pore size or the increase in fouled layer thickness. According to the analysis, the mean pore size of the fouled membrane, $d_{m,b}$, can be estimated using experimental resistance data and expressed as [16]:

$$d_{m,b} = \left(d_{m,o}^2 \frac{R_m}{R_f}\right)^{0.5} \tag{12}$$

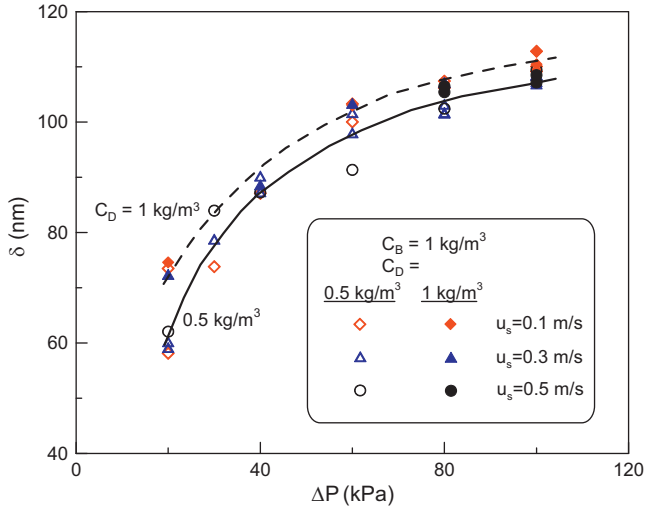

Fig. 13. A plot of δ versus ΔP under various operating conditions.

where $d_{m,o}$ is the mean pore size of the virgin membrane. Therefore, the dextran adsorption layer thickness, δ, can be calculated by $(d_{m,o} - d_{m,b})/2$.

Fig. 13 is a plot of δ versus ΔP under various operating conditions and two different dextran concentrations. The trend is similar to normal adsorption isotherms, in which the adsorption amount is proportional to the dextran concentration and applied pressure. This effect is more significant under low pressures or with a thin dextran adsorption layer. Moreover, the data for a given dextran concentration can be regressed to a unique curve whatever the cross-flow velocity. This result indicates that the dextran adsorption in the membrane pores is mainly determined by the dextran concentration and applied pressure. The empirical relationships obtained from Fig. 13 provide a way to predict membrane pore size reduction and membrane internal fouling directly from operating conditions.

4. Conclusions

The membrane fouling mechanisms in cross-flow microfiltration of BSA/dextran mixtures were studied. BSA aggregates deposited on the membrane surface to form a thin cake layer, while dextran molecules adsorbed in the pores near the membrane surface to narrow the pore size and result in a dominant filtration resistance. The BSA deposition was mainly determined by the drag forces exerted on the BSA aggregates. The cake mass increased linearly with increasing F_n/F_t force ratio. On the other hand, the dextran adsorption in the membrane pores was increased by the increases in dextran concentration and applied pressure, which was similar to most adsorption isotherms. The BSA and dextran concentration effects on the filtration flux and resistance were also discussed. The filtration fluxes for BSA/dextran mixtures decreased with increasing BSA or dextran concentration. However, the impact of the dextran concentration was more significant because the filtration resistance caused by membrane blocking was much higher than that caused by cake formation. The filtration resistances due to concentration polarization, cake formation and membrane internal fouling could be estimated directly from the operating conditions using the semi-theoretical methods proposed in this study.

Acknowledgements

The authors wish to express their sincere gratitude to the National Science Council of the Republic of China for its financial support. The assistance in CSLM measurement by Confocal Microscope Lab, Instrumentation Center, National Taiwan University, Taiwan is also appreciated.

References

[1] G. Belfort, R.H. Davis, A.L. Zydney, The behavior of suspensions and macromolecular solutions in crossflow microfiltration, J. Membr. Sci. 96 (1994) 1–58.
[2] E.M. Tracey, R.H. Davis, Protein fouling of track-etched polycarbonate microfiltration membranes, J. Colloid Interf. Sci. 167 (1994) 104–116.
[3] W.R. Bowen, J.I. Clavo, A. Hernández, Steps of membrane blocking in flux decline during protein microfiltration, J. Membr. Sci. 101 (1995) 153–165.
[4] I.H. Huisman, P. Prádanos, A. Hernández, The effect of protein–protein and protein–membrane interactions on membrane fouling in ultrafiltration, J. Membr. Sci. 179 (1–2) (2000) 79–90.
[5] C. Guëll, R.H. Davis, Membrane fouling during microfiltration of protein mixtures, J. Membr. Sci. 119 (2) (1996) 269–284.
[6] M. Ouammou, N. Tijani, J.I. Calvo, C. Velasco, A. Martín, F. Martínez, F. Tejerina, A. Hernández, Flux decay in protein microfiltration through charged membranes as a function of pH, Colloid Surf. A 298 (3) (2007) 267–273.
[7] E. Iritani, Y. Mukai, T. Murase, Upward dead-end ultrafiltration of binary protein mixtures, Sep. Sci. Technol. 30 (3) (1995) 369–382.
[8] M. Balakrishnan, G.P. Agarwal, Protein fractionation in a vortex flow filter. II. Separation of simulated mixtures, J. Membr. Sci. 112 (1996) 75–84.
[9] W.F. Blatt, A. Dravid, A.S. Michaels, L.M. Nelsen, Solute polarization and cake formation in membrane ultrafiltration, causes, consequences and control techniques, in: J.E. Flinn (Ed.), Membrane Science and Technology, Plenum Press, New York, USA, 1970, pp. 47–97.
[10] M. Cheryan, Ultrafiltration and Microfiltration Handbook, Technomic Publishing Co., Pennsylvania, USA, 1998, pp. 113–130.
[11] T.W. Cheng, H.M. Yeh, C.T. Gau, Resistance analyses for ultrafiltration in tubular membrane module, Sep. Sci. Technol. 32 (1997) 2623–2640.
[12] V. Garcia-Molina, S. Esplugas, Th. Wintgens, Th. Melin, Ultrafiltration of aqueous solutions containing dextran, Desalination 188 (2006) 217–227.
[13] A. Vernhet, M. Moutounet, Fouling of organic microfiltration membranes by wine constituents: importance, relative impact of wine polysccharides and polyphenols and incidence of membrane properties, J. Membr. Sci. 201 (1–2) (2002) 103–122.
[14] K.J. Hwang, P.S. Huang, Cross-flow microfiltration of dilute macromolecular suspension, Sep. Purif. Technol. 68 (2009) 328–334.
[15] H. Susanto, H. Arafat, E.M.L. Janssen, M. Ulbricht, Ultrafiltration of polysaccharide–protein mixtures: elucidation of fouling mechanisms and fouling control by membrane surface modification, Sep. Purif. Technol. 63 (3) (2008) 558–565.
[16] K.J. Hwang, P.Y. Sz, Filtration characteristics and membrane fouling in cross-flow microfiltration of BSA/dextran binary suspension, J. Membr. Sci. 347 (2010) 75–82.
[17] C.C. Ho, A.L. Zydney, A combined pore blockage and cake filtration model for protein fouling during microfiltration, J. Colloid Interf. Sci. 232 (2000) 389–399.
[18] J.S. Shiau, C.H. Tang, T.Y. Lin, D.M. Wang, A model for resistance growth during protein microfiltration, Sep. Sci. Technol. 38 (2003) 917–932.
[19] R.J. Hunter, Foundations of Colloid Science, vol. I, Oxford University Press, New York, USA, 1987 (Chap. 2).
[20] R. Kommedal, K. Milferstedt, R. Bakke, E. Morgenroth, Effects of initial molecular weight on removal rate of dextran in biofilms, Water Res. 40 (2006) 1795–1804.
[21] J. Hermia, Constant pressure blocking filtration laws – application to power law non-Newtonian fluid, Trans. Inst. Chem. Eng. 60 (1982) 183–187.
[22] W.M. Lu, S.C. Ju, Selective particle deposition in cross-flow filtration, Sep. Sci. Technol. 24 (7–8) (1989) 517–540.
[23] K.J. Hwang, K.P. Lin, Cross-flow microfiltration of dual-sized submicron particles, Sep. Sci. Technol. 37 (10) (2002) 2231–2249.
[24] J.D. Sherwood, The force on a sphere pulled away from a permeable half-space, Physicochem. Hydrodyn. 10 (1988) 3–12.